

# An Inter-Comparison of Two Independent Site Test Interferometers Located in Goldstone, California: Initial Study Results<sup>1</sup>

David Morabito and Larry D'Addario  
Jet Propulsion Laboratory  
California Institute of Technology  
Pasadena, California 91109  
USA

Roberto J. Acosta and James A. Nessel  
NASA Glenn Research Center  
21000 Brookpark Rd. MS 54-8,  
Cleveland, OH 44135  
USA

Phone: 818-354-2424, Fax: 818-394-6825, E-mail: [David.D.Morabito@jpl.nasa.gov](mailto:David.D.Morabito@jpl.nasa.gov)  
Phone: 818-393-0389, Fax: 818-393-2488, E-mail: [ldaddario@jpl.nasa.gov](mailto:ldaddario@jpl.nasa.gov)  
Phone: 216-433-6640, Fax: 216-433-8705, E-mail: [roberto.j.acosta@nasa.gov](mailto:roberto.j.acosta@nasa.gov)  
Phone: 216-433-2546, Fax: 216-433-8705, E-mail: [james.a.nessel@nasa.gov](mailto:james.a.nessel@nasa.gov)

## ABSTRACT

Site Test Interferometers (STIs) have been deployed at two different locations at the NASA Deep Space Network (DSN) tracking complex in Goldstone, California. An STI measures the difference in path length between a geostationary satellite and two antennas on the Earth, producing a measure of atmospheric phase fluctuations over spatial distances comparable to those between elements of possible microwave phased arrays. The purposes of the Goldstone STIs are to assess the suitability of Goldstone as an array site and to statistically characterize atmospheric induced delay fluctuations for application to future array scenarios.

The two STI's are separated by 13 km across the Goldstone complex. Each instrument is composed of two small-diameter antennas and associated electronics separated by ~200 meters in a principally east-west configuration. The antennas continuously observe signals emitted by geostationary satellites and produce data that contain information on the phase difference between signals received by both antennas. The fluctuation in delay (or path length difference) statistics derived from these data sets can be used to infer power loss for particular array configurations.

We report on a comparison of the RMS phase delay statistics estimated over 10-minute intervals between the two Goldstone STIs. We have achieved good statistical agreement between the data acquired from the two STIs, given that each instrument is observing different satellites, at different frequencies, over different baseline lengths, with very different implementations, and are located 13 km apart in widely separated terrain at different geodetic altitudes.

## 1. INTRODUCTION

The role of the atmosphere in degrading interferometric measurements for radio astronomy and multiple antenna element arrays has been discussed by several investigators cited in [1]. In order to assess such atmospheric effects at given sites, specialized instruments known as Site Test Interferometers (STI) have been utilized. An STI measures the difference in path length between a geostationary satellite and the two points on the Earth representing the spatial separation of the two antennas (or one baseline) of the STI.

The Goldstone Deep Space Communications Complex (DSCC) located in the Mojave Desert in California is being considered as a potential site for a future array of smaller diameter antennas that could replace the aging monolithic structures of the current Deep Space Network (DSN) [2]. An example of such an existing array in Goldstone would include the 34-m diameter beam waveguide (BWG) antenna subnet at X-band (7.15 GHz). STIs have been deployed at two of the three DSN complexes in Goldstone and Canberra in order to statistically characterize atmospheric decorrelation

---

<sup>1</sup> Copyright 2012. All rights reserved.

effects over typical antenna element separations of such an array. These instruments consist of at least two small-diameter outdoor antennas and associated electronics with element separations of ~200 meters with optical fiber (or coaxial) connections carrying LO and IF signals between each element, and an indoor electronics rack. The antennas continuously observe signals emitted by geostationary satellites and the phase difference of the received signals is measured. During post-processing, long period trends due to satellite motion and instrumental drift are removed. The resulting phase delay residuals contain fluctuations dominated by the troposphere on time scales ranging from ~1 second to several hundred seconds. An STI allows for the measurement of the difference in path length between a distant source and two points on the Earth, thereby providing a means of measuring these fluctuations over spatial distances comparable to those of the element separations of possible microwave phased array configurations.

The statistics of these delay fluctuations vary among sites due to climate and altitude, and at any one site diurnally, seasonally, and with passage of weather systems. It is desired to operate an STI for several years in order to establish a reliable statistical characterization of atmospheric decorrelation effects at a particular site. These data can thus be used to characterize the suitability of sites for hosting an uplink array, or their statistics can be used in link characterizations for current or proposed missions using the given array site. The statistics can be used to estimate phasing loss for a given array configuration by appropriate scaling of the STI's elevation angle, frequency, site altitude and antenna spacing to those of the array [3-7]. The STI data could also be used to provide real-time information on atmospheric effects when deployed next to an array being used for uplink when a downlink signal reference is not available, or the data can be used in scheduling tracks.

The first STI deployed in the Goldstone complex was at the Venus antenna site in May 2007 [4, 8], located next to the 34-m diameter DSN Research and Development (R&D) antenna designated DSS13: latitude of 35.07°N, longitude of 243.206°E and height above WGS84 ellipsoid of 1070.4 m [9]. Data acquisition for this STI began in May 2007. This instrument has a baseline separation of 256-m, and it observes the ANIK-F2 geostationary satellite with an orbital longitude of 111.1°W at an elevation angle of 48.5° at a frequency of 20.2 GHz. An unmodulated carrier tone in the spectrum of the transmitted signal from ANIK F2 serves as the signal source for the STI. The procedures used to analyze the acquired STI phase data are discussed elsewhere [8]. The phase of each antenna's received signal with respect to a local clock over each 1.0-s interval, and the difference of these measurements is the raw observable, which is unwrapped and filtered in 600-s blocks. In each block, the least-squares best-fit 2<sup>nd</sup> degree polynomial model is removed from the data, which filters out the long period non-tropospheric trends due to satellite motion and instrumental drift. The remaining fluctuations in the phase residuals are due to turbulence in the troposphere. The standard deviation of the residuals is then calculated for each block. An example on the use of the STI phase data in telecommunications link budgets was presented in *Morabito et al.* [2008] [10]. The results of the first year of phase stability measurements are presented in *Nessel, Acosta and Morabito* [2008] [4], which discusses analysis of the saturation RMS phase; the phase structure function exponent (used to transform the acquired data to other baselines); and the cumulative distribution function of the RMS phase. The deployment logistics and ongoing data analysis for the Venus STI were collaborative efforts between signal propagation experimenters at the Glenn Research Center (GRC) and Jet Propulsion Laboratory (JPL) NASA centers [4, 8, 11, and 12].

A second STI was deployed at the Apollo antenna site in Goldstone, California in September 2010 at latitude 35.16°N, longitude of 243.125°E and WGS height of 951.5 m [9]. The Apollo site is home to the operational beam waveguide (BWG) subnet of the DSN consisting of three 34-m diameter antennas. This subnet is a candidate for X-band uplink array activities and has been used for 7.15 GHz (X-band) uplink array demonstrations which suggested that atmospheric contributions to array amplitude loss are very small, (<< 1 dB) at that frequency [6,13-14]. The Apollo STI is located about 12.5 km away at a heading of 324° with respect to the Venus STI.

The Apollo STI design is that of an equal-arm white noise interferometer making use of a satellite's wideband digital TV broadcast signals. To a large extent, it is a copy of an earlier design by the Harvard-Smithsonian Center for Astrophysics (CfA) of the Submillimeter Array on Mauna Kea, Hawaii [15]. This design uses two (or more) 0.84-m diameter reflector antennas and associated electronics to receive the broadband signals emitted by the Ciel 2 geostationary broadcast satellite at an orbital longitude of 129°W, at an elevation angle of 47° and center frequency of 12.45 GHz. The received signals are mixed with LO signals carried on optical fiber from the central processor rack located within an environmentally-controlled building. The resulting IF signals are brought back to the indoor signal processing rack on separate optical fibers where they are cross-correlated using analog I-Q mixers that output in-phase (I) and quadrature-phase (Q) components of the cross power. The outputs of the IQ mixers are digitized and averaged over each 0.1 s interval; these are the raw

observables of the instrument which are recorded in real time to a local disk drive, and periodically downloaded via TCP/IP connections to other computers for further processing and analysis. Measurements from other instruments at the site (or nearby) are also downloaded, such as from water vapor radiometers (WVRs) and meteorology stations. In October 2011, a third element was added to the Apollo STI forming a three-baseline triangular array, which allows for characterization of two-dimensional tropospheric effects. A three-element STI of the same design is also operating at the DSN tracking site near Canberra, Australia. However, this paper will report only on the inter-comparison between the originally deployed east-west Goldstone Apollo STI baseline and that of the Goldstone Venus baseline which is also oriented in a predominantly east-west direction. We will present results of the phase delay statistics extracted from these two independent Goldstone STIs as well as quantify the relative performance of these two widely spaced STIs. The comparison of these two independent STIs provides important data that will help assess the suitability of the Goldstone site to support widely distributed antenna systems for future RF and optical communications. For a more comprehensive treatment of the results of this study, the reader is referred to [16].

## 2. GENERATION OF PATH DELAY STATISTICS

The fundamental observable of the STI is the phase difference (or correlation phase),  $\phi(t)$ , between the individual elements of an interferometer of length  $r_{sti}$  pointed at a geo-stationary satellite emitting a signal at frequency  $f_{sti}$ , (either a carrier tone or center of a wideband signal) and located at a local elevation angle of  $\theta_{sti}$  in the sky. These phase differences are measured differently for the two different designs of STIs. The sampling interval of the time series from the Venus STI is  $\Delta t = 1$  s and for the Apollo STI it is 0.1 s. This phase for a one day period exhibits a diurnal signature due to satellite motion as the satellite is located within the beam of each fixed antenna element. The geostationary satellite is restricted to lie within a fixed “box” in the sky whose dimensions are smaller than the beamwidth of each antenna.

The data from the Venus and Apollo STIs are closely examined and compared to evaluate the relative performance and consistency of the measurements. The Venus STI measures in-phase (I) and quadrature-phase (Q) components of the baseband signal every 1.0 s with respect to the receiver's LO, separately for each antenna. The Apollo STI measures the in-phase (I) and quadrature-phase (Q) cross-correlation of its two IF signals every 0.1 s.

During post processing, the 4-quadrant phase angle  $\text{atan}(Q,I)$  is computed for each case; for the Venus STI, the phases of the two antennas are subtracted. During post-processing, the phase data are conditioned (to correct for cycle ambiguities) and filtered (to remove long period trends) [8]. A 2<sup>nd</sup> degree polynomial model is fit over each 600-sec block of data to estimate the contributions of long period satellite motion and instrumental drift. The instrumental drift in the phase includes slow variations due to environmental disturbances and component aging. The fitted model is subtracted from the data, and the resulting residuals  $\Delta\phi(t)$  are presumed to be dominated by the troposphere.

The statistics of the phase residuals  $\Delta\phi(t)$  are generated over intervals of  $T = 600$ -seconds for this study. This time interval was selected for routine Venus STI (element spacing of 256-m) data processing based on a rationale presented in [8]. Given that the Apollo STI has a similar element spacing (191-m), the use of 600-s blocks for Apollo data was deemed reasonable to facilitate comparison using equal duration blocks.

The fluctuations are characterized by the standard deviation of the residual phase over each 600-sec block of data ( $\sigma_{\Delta\phi}$ ). The level of and variation in  $\sigma_{\Delta\phi}$  are typically smaller during quieter cooler nighttime and winter periods and are typically larger during daytime and summer periods when the atmosphere is warmer and exhibits increased variability due to water vapor. The highest values of  $\sigma_{\Delta\phi}$  are expected to be measured during hot summer days and the lowest values are expected to be measured during cold winter nights.

To facilitate comparison of atmospheric conditions of widely separated STI instruments residing at the same site or between STIs residing at different sites, the results from each site can be translated to statistics that would be measured under standardized conditions. The line-of-sight  $\sigma_{\Delta\phi}$  RMS phase measurements from each STI are converted to zenith RMS delay  $\sigma_{\Delta\tau}$  by making the appropriate scaling in frequency, elevation angle, antenna element spacing, and WSM height to facilitate comparison as described below. Because the troposphere is non-dispersive, the present observations (20.2 GHz for the Venus STI and 12.5 GHz for the Apollo STI) can be scaled to higher or lower frequencies such as those used for deep space communications links (7.2 and 32–40 GHz).

The RMS phase for each STI is converted to a frequency-independent quantity by converting its scatter (standard deviation) at frequency  $f_{sti}$  to RMS delay at each sample time  $t_k$  [5]. The resulting

RMS delay is then also referenced to a common 90° elevation angle (zenith) by correcting for air mass at each STI elevation angle,  $\theta_{sti}$ , resulting in a zenith delay fluctuation [5]

$$\sigma_{\Delta\tau_z}(t_k; \theta = 90^\circ; r_{sti}) = \frac{\sigma_{\Delta\phi}(t_k)}{2\pi f_{sti}} (\sin \theta_{sti})^\gamma$$

where  $\gamma$  is an exponent whose value depends on the relationship between the height of the turbulent layer  $H$  and the baseline distance  $r_{sti}$ . Thus  $\gamma$  will be equal to  $1/2$  for  $r_{sti} \ll H$  (thick layer limit, short distance structure) and will be equal to 1 for  $r_{sti} \gg H$  (thin layer limit, long distance structure). This result conforms to the concept that the path will be dominated by many small sized irregularities for baseline sizes much smaller than the turbulent layer height (thick layer limit) and that the path will be dominated by fewer larger sized irregularities for baseline sizes much larger than the turbulent layer height (thin layer limit) [17].

These results can be scaled to a common element separation making use of the structure function dependence with baseline length. We choose to scale the Venus STI length  $r_{Venus}$  to that of the Apollo STI length  $r_{Apollo}$ . This scaling takes on the following form:

$$\sigma_{\Delta\tau_z}^2(t_k; \theta = 90^\circ, r_{Apollo}) = \sigma_{\Delta\tau_z}^2(t_k; \theta = 90^\circ, r_{Venus}) \left( \frac{r_{Apollo}}{r_{Venus}} \right)^\beta$$

The Kolmogorov theory of turbulence predicts this form with  $\beta=5/3$  for the thick-screen model, and  $\beta=2/3$  for the thin-screen model [18].

A height dependent scaling makes use of the assumption that the path delay variations are proportional to path delay which is in turn proportional to the integrated refractivity along the signal path. The refractivity is dependent upon the pressures of dry air and of water vapor. We assume that in the general case, the altitude dependence of these are roughly exponential although for the case of water vapor the lower portion of the atmosphere may be mixed especially during turbulent conditions. This scaling is further discussed elsewhere [16].

### 3. DIURNAL VARIATION OF RMS DELAY

The zenith RMS delay ( $\sigma_{\Delta\tau}$ ) referred to a common STI can be compared between STIs residing at the same site, and be examined on a monthly basis as well as between day and night, between seasons or from year to year. Cumulative distributions of the zenith delay fluctuation measurements,  $\sigma_{\Delta\tau}$ , can also be generated in tabular form and be prepared for future publications such as for the DSN's 810-005 Telecommunications Link Control Document [19]. The information from such tables would be used in spacecraft-to-ground telecommunications link budget calculations involving a particular array configuration on the ground. The statistics can then be translated to the link frequency and elevation angle of interest and scaled to the baseline of each element pair in an array and thus be used to predict array loss for particular array configurations.

The time series of the residual RMS delay over each 600 second block for the month of December 2011 is shown in Figure 1. These data are representative of a "quiet" month marked by less turbulent conditions. The data for the warm summer month of August 2011 is shown in Figure 2. Here there is more variation between the reasonably quiet nighttime conditions and larger fluctuations occurring during daytime. The scatter of the RMS delay measurements over all the blocks for the colder month December 2011 is much smaller than that for the warmer month August 2011.

Upon examination of Figures 1 and 2, it is apparent that the time series of the delay statistics from the Apollo STI and Venus STI follow each other very well during quiet conditions, and reasonably well during daytime periods of higher turbulence with any differences likely attributable to terrain and local weather conditions. These two instruments are separated by 12.5 km and each is located in terrain with different surrounding topographical features. Thus the temporal  $\sigma_{\Delta\tau}$  signatures from the two STIs follow each other reasonably well given the distance between them, providing insight the applicability on the use of such statistics over a wide region of similar terrain and climate. It should be noted that the data sets plotted in Figures 1 and 2 have an additional contribution of about 0.1 ps of RMS delay due to instrumental noise, which is considered negligible. Plots involving multiple STI data sets from independent STIs residing at nearby sites such as these shown in Figures 1 and 2 provide confidence and validation checks for the data sets as well as being useful during periods of major differences such as revealing passage of atmospheric structures (via correlation with prevailing wind) or for revealing instrumental anomalies.

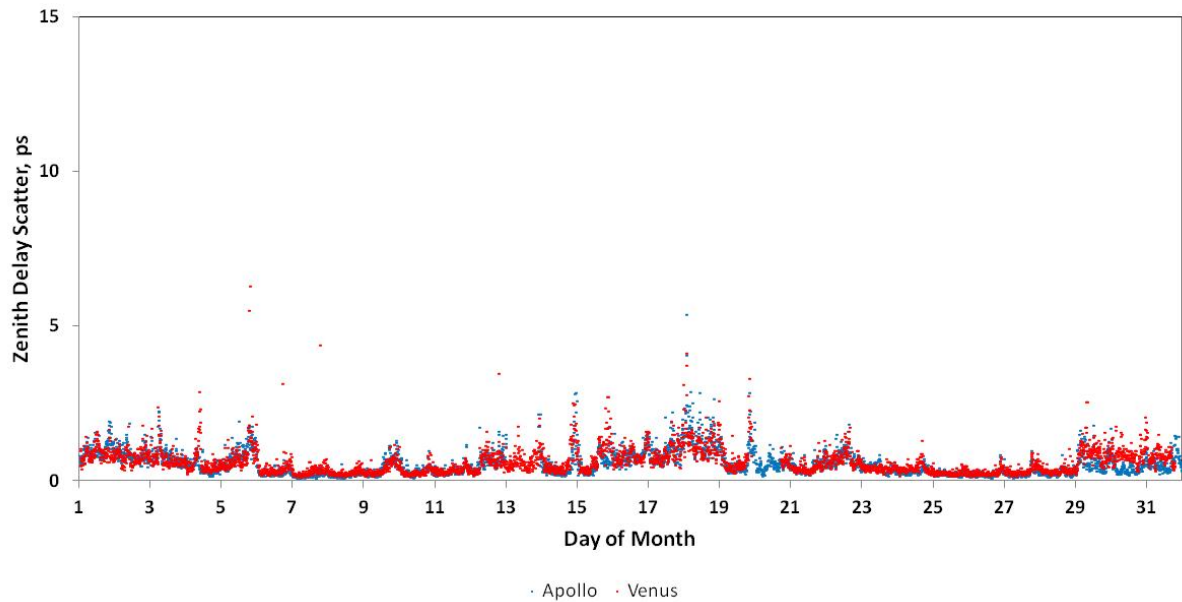


Figure 1 – December 2011 zenith RMS delay over 600-s time intervals (blue points denote Apollo STI values, red points denote Venus STI values).

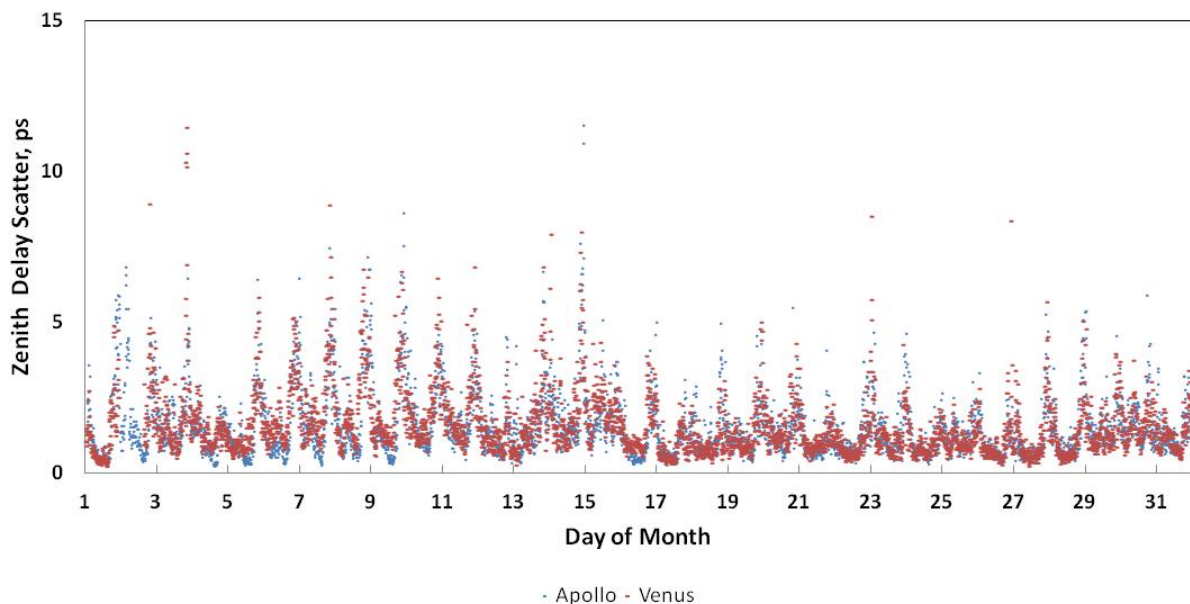


Figure 2 – August 2011 zenith RMS delay over 600-s time intervals (blue points denote Apollo STI values, red points denote Venus STI values).

#### 4. SEASONAL VARIATION OF RMS DELAY

More than a year of common data between the two Goldstone STIs were acquired since September 2010 when the Apollo STI was first installed. In this paper we will focus on data acquired between January 2011 and January 2012.

The statistics for several months of zenith delay data for the Apollo and Venus STIs are summarized in Figure 3 which displays minimum, maximum and average standard deviations among all 600-s blocks for each month after the standardizations discussed in Sec. 2 were performed. The minimum scatter,  $\sim 0.1$  ps, is believed to lie near the instrumental thermal noise limit for each STI. The average values are very close in magnitude providing evidence that the statistics are in reasonable agreement for the Goldstone complex despite the two instruments being located 13 km apart in differing terrain. The maximum values are also in generally good agreement. Although one

does not expect the time series of the RMS delay to always agree, especially during turbulent weather conditions such as during passage of weather fronts and consequent terrain effects, their statistics over time appear to be reasonably consistent.

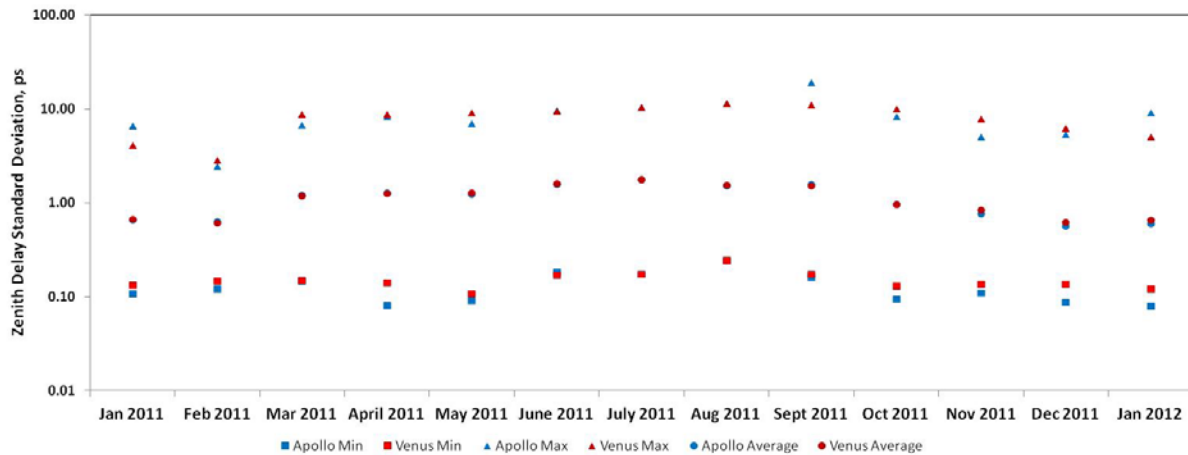


Figure 3 – Minimum, average, and maximum STI zenith RMS delay over the data acquired each month from the Apollo and Venus east-west STIs.

The minimum zenith RMS delay for the Venus STI typically was ~0.16 ps, which is in agreement with that measured from the zero baseline tests performed in Cleveland [11] prior to shipment and deployment of the equipment to Goldstone. The Apollo STI RMS delay has a generally lower minimum value than that of the Venus STI due primarily to its higher SNR intrinsic with the nature of the Ciel 2 wideband signal and subsequent processing.

## 5. CUMULATIVE DISTRIBUTION OF ZENITH RMS DELAY

We examine monthly cumulative distributions of the normalized zenith RMS delay over 600-s blocks from each STI and perform the subsequent inter-comparison. Figure 4 displays the monthly cumulative distribution curves of the zenith RMS delay statistic gathered from both the Apollo and Venus STIs at Goldstone for the period from April 2011 to January 2012. The distributions of the warmer months (summer) are shown in reddish colors and the curves for the cooler months (winter) are shown in bluish colors. The curves for the intermediate months (spring and autumn) are shown in greenish-yellowish colors. As expected, the curves for the warmer months (when there are higher fluctuations due to higher temperature and more turbulence) lie on the right side of the plot, while those of the cooler months (when temperature is lower and turbulence is less) lie on the left side of the plot. The CDF curves for the spring-autumn months generally lie in between those of the warm and cool months.

We also note that the individual month curves for each STI (Apollo solid curves and Venus dashed curves in Figure 4) follow each other fairly well after applying all of the adjustments discussed in Sec. 2. However, there are a few notable differences between STI curves such as for January 2012 at intermediate cumulative distribution values (light purple in Figure 4) and for July 2011 for low cumulative distribution values (red curves in Figure 4). These small differences may be due to terrain differences coupled with wind patterns at each site, as one possible explanation.

The STI data from two widely spaced locations are thus expected to be in general statistical agreement but any differences in their temporal signatures could be associated with the passage of weather systems and effects of terrain. When examining the time series of the standard deviations of the path delays over 600-second periods ( $\sigma_{\Delta\phi}$ ) between spatially separated STIs one expects better agreement during cooler quiet periods such as night-time and winter, and larger differences between the two data sets during warmer more turbulent weather conditions such as during summer days. During warmer periods, large differences between the data sets are expected to be due to effects of local terrain coupled with differences in local weather (different wind speeds and directions) that may impact the observations in different ways. One also expects to occasionally see the delayed effects of large storm cells as they propagate over the complex. Such effects can be correlated with local weather data (e.g., wind speed and direction) and nearby WVR data (e.g., path delay).

Good agreement has been demonstrated between the monthly cumulative distribution curves of the Apollo and Venus STIs that lie within the same climatic region (~13 km apart) after making adjustments for frequency, elevation angle, baseline length and altitude. These results provide insight on the use of such data to evaluate potential array locations. By referencing the statistics for multiple

STIs from different sites to a common parameter set, one can better make comparisons on the local climate's impact on array performance. Such results can be used by telecom system designers in considering climate as well as geometry and other factors for selection of potential array sites.

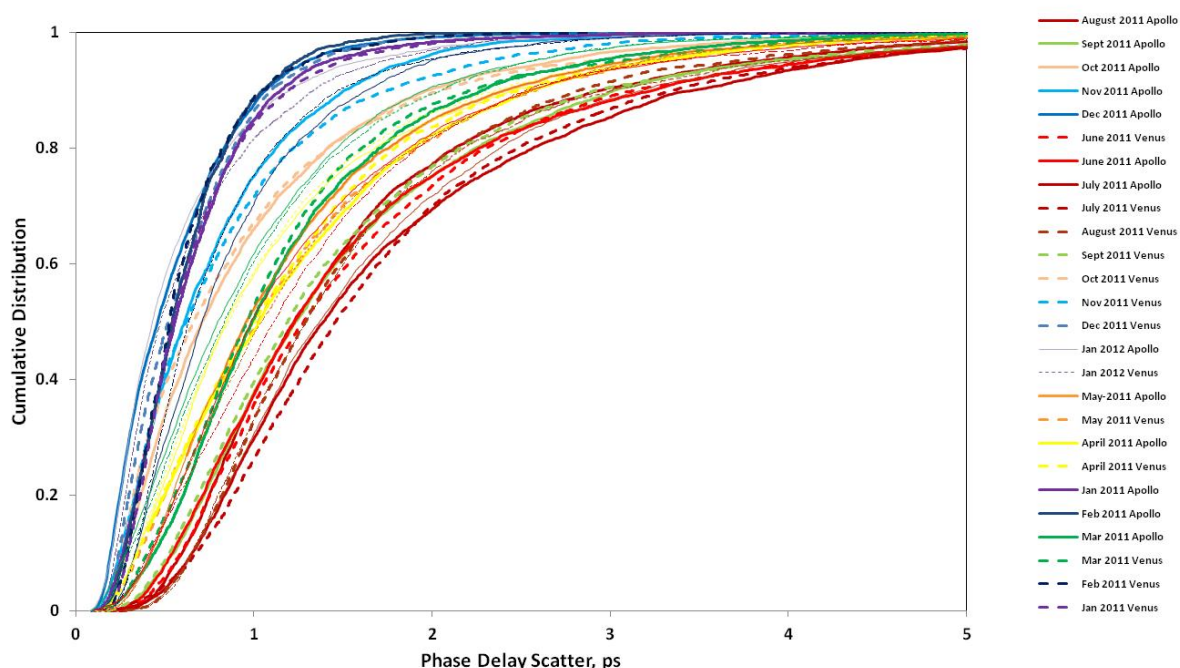


Figure 4 – Cumulative distribution of STI zenith RMS delay in 600-sec blocks for each month.

## 6. ARRAY LOSS CALCULATED FROM RMS PHASE DELAY

Atmospheric delay fluctuations over an element spacing of an array cause variations in the transmitted power of the uplink array as seen from a spacecraft. Discussion on scenarios and different approaches in estimating telemetry loss for an uplink array has been presented elsewhere [3]. A reasonable link budget can be constructed by using the mean value of loss (under a given set of conditions) along with the nominal values of other link parameters, and then considering a range of adverse and favorable variations from the mean using methodology available in the literature [20]. A more comprehensive treatment of the array loss extracted from the data in this study can be found in [16].

## 7. CONCLUSION

Site Test Interferometers (STIs) have been deployed at the Venus and Apollo antenna sites in Goldstone, California to assess the suitability of Goldstone as an uplink array site, and to statistically characterize atmospheric induced phase fluctuations for application to potential Goldstone array link scenarios. We have presented preliminary results of an inter-comparison of the delay statistics extracted from these two independent instruments. Both STIs have been shown to produce approximately equivalent results after adjusting for differences in their geometries. The comparison of the two independent STIs provides important data that will help assess the suitability of the site to support widely distributed antenna systems for future Ka-band and optical communications. The delay statistics can be used to estimate array loss that can be used in telecommunications link budgets involving phased arrays.

## 8. ACKNOWLEDGEMENTS

We acknowledge and appreciate the assistance and cooperation of the NASA Deep Space Network and the DSS-13 station crew. We want to thank Faramaz Davarian, Steve Townes, and Barry Geldzahler for support of this work. Most of the design of the Apollo station STI was copied from the phase monitoring system of the Sub-Millimeter Array on Mauna Kea, Hawaii, developed at the Harvard-Smithsonian Center for Astrophysics. We are grateful to Robert Kimberk, Steve Leiker, John Test, and Ray Blundell of CfA for sharing their detailed design information and software. The research described in this paper was carried out at the Jet Propulsion Laboratory, California Institute of Technology, under a contract with the National Aeronautics and Space Administration.

## 9. REFERENCES

- [1] Zheng, Y., J. P. Basart, and Y. Koh (1990), Correcting atmospheric-induced phase errors of a synthetic aperture antenna array by time series modeling and Kalman filtering, *Radio Sci.*, 25(6), 1145–1158, doi:10.1029/RS025i006p01145.
- [2] Davarian, F., "Uplink Arrays for the Deep Space Network", (2007), Proc. of the IEEE, Vol 95, Issue 12.
- [3] Morabito, D. D. and L. D'Addario, "Two-Element Uplink Array Loss Statistics Derived from Site Test Interferometer Phase Data for the Goldstone Climate: Initial Study Results," IPN PR 42-186, pp. 1-20, August 15, 2011.
- [4] Nessel, J. A., Acosta, R. J., and Morabito, D. D., "Phase Fluctuations at Goldstone Derived from One Year Site Testing Interferometer Data", *Proceedings of the 14th Ka and Broadband Communications Conference*, September, 2008, Matera, Italy.
- [5] Morabito, D. D., and D'Addario, L., "Site Test Interferometer Atmospheric Decorrelation Statistics Use in Uplink Array Link Budgets" *Proceedings of 13th Ka and Broadband Communications Conference*, September 24-26, 2007, Turin, Italy.
- [6] D'Addario, L., "Estimates of Atmosphere-Induced Gain Loss for the Deep Space Network Array", *InterPlanetary Network Progress Report 42-160*, February 15, 2005.
- [7] L. R. D'Addario, "Combining Loss of a Transmitting Array due to Phase Errors," IPN PR 42-175, pp. 1-7, November 15, 2008.
- [8] Acosta, R. J., Nessel, J. A., and Morabito, D. D., "Data Processing for Atmospheric Phase Interferometers", *Proceedings of the 14th Ka and Broadband Communications Conference*, September, 2008, Matera, Italy.
- [9] Kwok, A., "Coverage and Geometry", Module 301 Rev. F in the DSN Telecommunications Link Design Handbook 810-005 Rev. E., Released June 1, 2010
- [10] D. D. Morabito, L. D'Addario, S. Shambayati, R. J. Acosta, and J. A. Nessel, "Goldstone Site Test Interferometer Atmospheric Decorrelation Statistics use in Spacecraft Link Budgets: First Year of STI Data", *Proceedings of the 14th Ka and Broadband Communications Conference*, September 24-26, 2008, Matera, Italy.
- [11] Acosta, R. J., Frantz, B., Nessel, J. A., and Morabito, D. D., "Goldstone Site Test Interferometer", *Proceedings of the 13th Ka and Broadband Communications Conference*, September 24-26, 2007, Turin, Italy.
- [12] Nessel, J. A., Acosta, R. J., and Morabito, D. D., "Goldstone Site Test Interferometer Phase Stability Analysis", *Proceedings of the 13th Ka and Broadband Communications Conference*, September 24-26, 2007, Turin, Italy.
- [13] V. Vilnrotter, D. Lee, T. Cornish, P. Tsao, L. Paal, V. Jamnejad, "Uplink Array Concept Demonstration with the EPOXI Spacecraft", *Proceedings of the 2009 IEEE Aerospace Conference* held in Big Sky, Montana, March 7-14, 2009, paper 4.0101.
- [14] Vilnrotter, V., D. Lee, T. Cornish, R. Mukai, and L. Paal, "Uplink Arraying Experiment with the Mars Global Surveyor Spacecraft," IPN PR 42-166, pp. 1-14, August 15, 2006.
- [15] R. Kimberk, S. Leiker, J. Test, R. Wilson, and T. Hunter, "The Submillimeter Array Atmospheric Phase Monitor" *SMA Newsletter*, No. 9, pp 9-10, January 28, 2010. Available: <http://www.cfa.harvard.edu/sma/newsletter/smaNews28Jan2010.pdf>
- [16] D. D. Morabito, L. D'Addario, S. Shambayati, R. J. Acosta, and J. A. Nessel, "An Inter-Comparison of Two Independent Site Test Interferometers Located in Goldstone, California", *IEEE TAP* (submitted)
- [17] Treuhaft, R. N. and Lanyi, G. E., "The effect of the dynamic wet-troposphere on radio interferometric measurements", *Radio Science*, Vol. 22, No. 2, pp. 251-265, March-April, 1987.
- [18] Coulman, C., "Fundamental and applied aspects of astronomical seeing." *Ann. Rev. of Astron. and Astrophys.*, Vol. 23, pp. 19-57, 1985.
- [19] Slobin, S., "Atmospheric and Environmental Effects", Module 105 Rev. D in the DSN Telecommunications Link Design Handbook 810-005 Rev. E., Released September 15, 2009
- [20] Yuen, J. H. Ed., *Deep Space Telecommunications Systems Engineering*, Plenum Press, New York, 1983.